

Communication

Preparation and Gas Separation of Amorphous Silicon Oxycarbide Membrane Supported on Silicon Nitride Membrane

Hengguo Jin and Xin Xu *

CAS Key Laboratory of Materials for Energy Conversion, Department of Materials Science and Engineering, University of Science and Technology of China, Hefei 230026, China; jhg@mail.ustc.edu.cn

* Correspondence: xuxin@ustc.edu.cn

Abstract: An amorphous silicon oxycarbide membrane supported on a silicon nitride membrane substrate was prepared. A starting suspension containing polyhydromethylsiloxane (PHMS), tetramethyltetravinyl-cyclotetrasiloxane (TMTVS) and a platinum catalyst was first prepared and spin-coated on a silicon nitride membrane, and then the suspension was cross-linked and cured, followed by pyrolyzing at 1000 °C under a flowing Ar atmosphere. A dense amorphous silicon oxycarbon ceramic membrane with a thickness of about 1.8 μm was strongly bonded to the Si₃N₄ membrane substrate. The single gas permeation of H₂ and CO₂ indicated that the ideal permeation selectivity of H₂/CO₂ was up to 20 at 25 °C and 0.5 MPa with good long-term stability, indicating the potential application of the obtained membrane for hydrogen purification.

Keywords: silicon oxycarbide; silicon nitride; pre-ceramic polymers; spin coating; pyrolysis; gas separation

1. Introduction

With an ever-evolving society, the world is facing energy and climate issues [1], which urgently need to be resolved. As a renewable, non-toxic gas [2], hydrogen has a high calorific value [3] and does not produce greenhouse gases [4], so it has a wide range of applications in energy and climate issues [5]. The production of hydrogen gas has gained great attention [6–11], while the purification of hydrogen is also a problem worthy of attention [12–14].

Hydrogen purification methods are mainly pressure swing adsorption [15–18], cryogenic distillation [13,19] and membrane separation [20]. Compared with the other two methods, the membrane separation method has received more and more attention due to its simple operation [21], low energy consumption [22–24], low investment cost [25] and high efficiency [26,27]. Many membranes have been studied [28], such as graphene oxide (GO) [29,30], polymers [31–35], pure metal membranes [28], mixed-matrix membranes [28] and zeolitic imidazolate frameworks (ZIFs) [36–40]. The porous structure of carbon membranes partially collapses at high temperatures [28]. Polymer membranes have low mechanical strength, are not resistant to corrosion and are highly sensitive to compaction [13]. The appearance of hydrogen embrittlement will cause cracks on the surface of metal membranes [28]. In mixed-matrix membranes, most fillers are expensive, and further study on the scaling up of the processes from the lab scale to the pilot scale is needed [28]. And the thickness of defect-free ZIF membranes used for separation is often very thick [36]. On the contrary, inorganic membranes are gaining more and more attention due to their excellent mechanical strength [41], strong corrosion [42] and high temperature resistance. Polymer-derived ceramics, such as SiOC, SiCN and SiOCN, have attracted great interest due to their low-temperature ceramization, molecular design, good manufacturability and processability [43–45].

In polymer-derived SiOC membranes, the SiOC network is generated by the substitution of two divalent oxygen ions by one tetravalent carbon ion within the SiO₂ network.



Citation: Jin, H.; Xu, X. Preparation and Gas Separation of Amorphous Silicon Oxycarbide Membrane Supported on Silicon Nitride Membrane. *Membranes* **2024**, *14*, 63. <https://doi.org/10.3390/membranes14030063>

Academic Editor: Mohamed Khayet

Received: 22 January 2024

Revised: 23 February 2024

Accepted: 27 February 2024

Published: 2 March 2024



Copyright: © 2024 by the authors. Licensee MDPI, Basel, Switzerland. This article is an open access article distributed under the terms and conditions of the Creative Commons Attribution (CC BY) license (<https://creativecommons.org/licenses/by/4.0/>).

CSi_4 units are locally formed to strengthen the network. They are most widely studied due to their low cost, high ceramic yield, moderate pyrolysis temperature and ease of control over curing and molding [46,47].

Many studies on SiOC have been carried out, such as the use of polymer-derived SiOC ceramic membranes for oil–water separation and membrane distillation [48], and polymer-derived SiOC microbeads have been used to make anodes for high-performance lithium-ion batteries [49]. SiOC was formed by pyrolysis using polyhydromethylsiloxane (PHMS) and tetramethyltetravinylcycletetrasiloxane (TMTVS) as the precursors of Si, which was amorphous, where oxygen and carbon were simultaneously connected to silicon. Generally, the application was mainly carried out by loading the precursor membrane layer on a traditional ceramic membrane support [50]. Prasad et al. [13] used vinyl-functionalized polysiloxane XP RV 200 as the precursor and successfully prepared an amorphous SiOC membrane on the substrate of an alumina tube by a dip coating method.

In this study, we successfully prepared an amorphous silicon oxycarbide membrane supported on a silicon nitride ceramic membrane substrate because silicon nitride has similar chemical bonds with SiOC, which was beneficial for uniform growth and the strong adhesion of the obtained SiOC membrane. The Si_3N_4 membrane contained large, straight finger-like voids, which favored the flow of gas. The prepared membrane showed good performance in the selective permeability of hydrogen and carbon dioxide.

2. Materials and Methods

Polyhydromethylsiloxane, 1,3,5,7-tetramethyl-1,3,5,7-tetravinylcyclo-tetrasiloxane and platinum divinyl-tetramethyl-disiloxane complex (Pt-C) were all purchased from Shanghai Guiyou New Material Technology Ltd., Shanghai, China. High-purity argon and nitrogen (greater than or equal to 99.999%) were from Nanjing Shangyuan Industrial Gas Factory.

A silicon nitride ceramic membrane with a diameter of 2.5 cm and a thickness of 1 mm was prepared by phase-inversion tape casting and pressureless sintering [51]. The Si_3N_4 membrane was polished with sandpaper, followed by washing with a hot sodium hydroxide solution [52]. The cleaned silicon nitride membrane was firmly fixed on a suction cup.

The preparation process for the ceramic separation membrane is shown in Figure 1a. PHMS (the precursor polymer) and TMTVS (the crosslinking agent) with a mass ratio of 1:1 were first mixed in a magnetic stirrer for one hour. Then, the Pt-C catalyst (1wt% of PHMS and TMTVS) was added and stirred for half an hour to make the hydrosilylation of Si-H and $\text{CH}_2=\text{CH}_2$ groups from PHMS and TMTVS more thorough, as shown in Figure 1b. The starting suspension was rotationally sprayed onto a silicon nitride membrane using an EZ4 spin coat (EZ4-S, Lebo Science, Wuxi, China), which rotated at 400 r/min and dropped 2 mL each time, followed by curing at a constant temperature in a humidity box (HSB-80L, Hefei Anke Environmental Testing Equipment Co., Ltd., Hefei, China). Subsequently, the ceramic membrane was heated in an oven at 80 °C for 12 h and then at 120 °C for another 12 h, and the polymeric gel was cross-linked. Afterward, the resulting PSO gel (cross-linked curing from PHMS, TMTVS and Pt-C) was pyrolyzed at different temperatures between 500 and 1000 °C in a flowing argon atmosphere for 3 h with a heating rate of 5 °C/min. The above procedure was repeated once to obtain the composite membrane.

The crystalline phases were identified by X-ray diffraction (XRD, Philips, PW 1700, Eindhoven, Netherlands). The cross-section and surface morphology of the final membrane were measured with a scanning electron microscope (SEM, JEOL JSM—6390LA, Tokyo, Japan), equipped with an EDS device for elemental analysis. The pyrolysis behavior was also examined through a differential scanning calorimetry–thermogravimetric analysis (DSC-TGA, SDT Q600, TA Instruments, New Castle, DE, USA) under a nitrogen atmosphere. The binding energies were characterized by X-ray photoelectron spectroscopy (XPS, Kratos Axis supra, Shimadzu, Kyoto, Japan). The specific surface areas and pore-size distributions of the ceramics were determined by a N_2 adsorption–desorption technique using an ASAP 2460 V3.00H instrument. Fourier transform infrared spectroscopy (FTIR, Nicolet6700,

Thermo Fisher, Waltham, MA, USA) was used to characterize the chemical bonds in polymer gels.

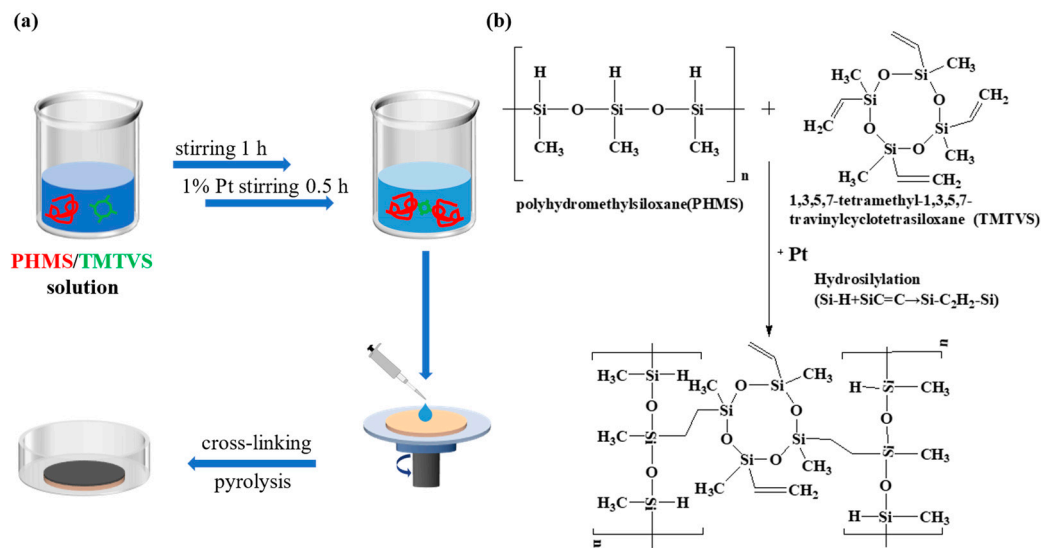


Figure 1. (a) Preparation diagram of composite ceramic membrane. PHMS and TMTVS correspond to the red and green lines, respectively. (b) Schematic diagram of the hydrosilylation reaction between PHMS and TMTVS.

The separation device and test method for a single gas were reported previously [36]. The test instrument is shown in Figure 2. The pressure difference between the feed side and the permeate side of the membrane was 0.5 MPa. The single H₂ (0.29 nm) and CO₂ (0.33 nm) gas permeability was measured as a function of time at 25 °C, and the ideal gas separation factor of H₂ and CO₂ was the ratio of the permeability of the two gases.

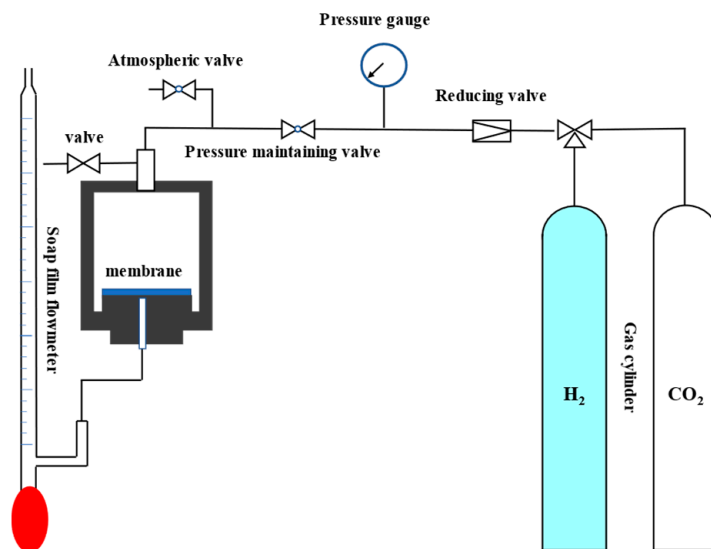


Figure 2. Gas permeation test equipment for the prepared ceramic membrane.

3. Results

3.1. Characterization of SiOC Ceramics

The DSC-TG analysis of the PSO gel was carried out in a nitrogen atmosphere, as shown in Figure 3a. The gel started to decompose at around 500 °C, suggesting a high level of stability in the gelling process [49]. The pyrolysis curve showed that a strong weight loss occurred in the temperature range of 500 to 800 °C, which might be due to the release of

low-molecular-weight oligomers, such as hydrogen, methane, etc. The strong exothermic peak close to 780 °C indicates the transition from the PSO gel to SiOC ceramics. The total weight loss indicated that the ceramic yield was about 83% at 1000 °C [49].

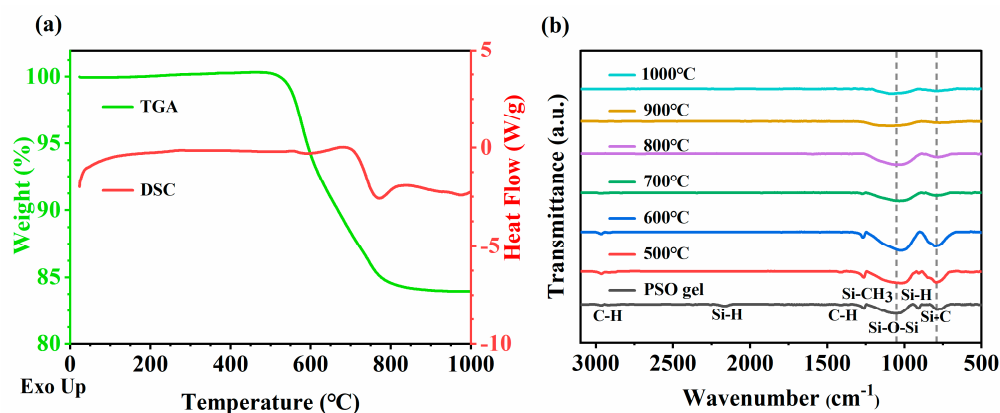
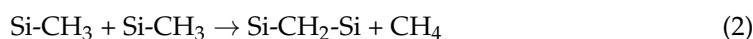


Figure 3. (a) The DSC-TG analysis of PSO gel. (b) Fourier transform infrared spectroscopy (FTIR) of PSO gel before and after pyrolysis at different temperatures.

Figure 3b shows the FTIR spectra after pyrolysis at different temperatures. There are always characteristic absorption peaks at approximately 790 cm⁻¹ and 1050 cm⁻¹, which were attributed to the stretching vibration of the Si-C bond and Si-O-Si bond, respectively. It is worth mentioning that Si-O-Si characteristic peaks always move in the direction of low wave number after pyrolysis. The PSO gel has peaks at 2960 cm⁻¹, 2160 cm⁻¹, 1410 cm⁻¹, 1260 cm⁻¹ and 910 cm⁻¹, corresponding to the characteristic absorption peaks of C-H, Si-H, C-H, Si-CH₃ and Si-H bonds, respectively. No absorption peak of the C=C bond was seen near 1600 cm⁻¹ because the C=C bond in TMTVS reacted with the Si-H bond in PHMS to form a Si-CH₂-CH₂-Si bond, which was completely consumed. Si-H disappeared at temperatures lower than 600 °C through the following equation [31]:



As the temperature increased, the peak of Si-CH₃ gradually decreased and disappeared at 800 °C through Equation (2):



A further condensation reaction of methylene was expected to occur at high temperatures, leading to the formation of a three-dimensional network structure and the release of CH₄.

Figure 4a presents the XPS analysis of the PSO gel and the SiOC membrane pyrolyzed at 1000 °C, where the photoelectron energy absorption peaks of Si, O and C could be detected. As shown in Figure 4b, the Si2p peak of the SiOC membrane can be decomposed into two peaks, namely 104.0 eV and 103.3 eV, attributed to the Si-O and Si-C bonds, respectively, which is in good agreement with the FTIR absorption spectrum (Figure 3b). Compared with the PSO gel, the SiOC ceramics exhibited a significantly decreased intensity of Si-C bonds, which could be attributed to the dissociation of Si-C [53].

Figure 5 shows the XRD diagram of the SiOC membrane pyrolyzed at 1000 °C and 1100 °C. When the treatment temperature was increased to 1100 °C, small graphite peaks appeared, indicating the decomposition of SiOC, while all the membranes obtained at temperatures lower than 1000 °C were amorphous [54].

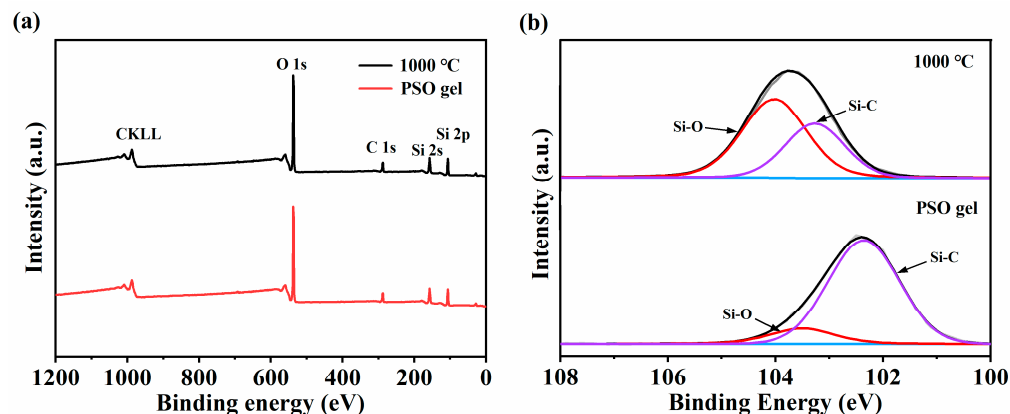


Figure 4. (a) XPS spectrum of PSO gel and SiOC membrane pyrolyzed at 1000 °C. (b) XPS fitting curve of Si2p.

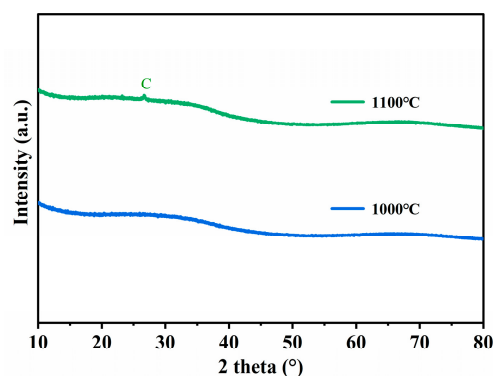


Figure 5. XRD diagrams of SiOC membrane pyrolyzed at 1000 °C and 1100 °C.

Figure 6a presents the SEM image of the cross section of the SiOC membrane on the Si_3N_4 ceramic membrane. The flat silicon nitride ceramic membrane revealed the existence of finger holes, which could significantly reduce the gas flow resistance. Figure 6a also shows the presence of pore penetration in the composite membrane, which can enhance the adhesion between the separation layer and the support layer through mechanical interlocking [55]. Figure 6b,c show the fracture and upper surface of the SiOC membrane. It can be clearly seen that a uniform and smooth SiOC membrane with a thickness of approximately 1.8 μm was successfully deposited on the surface of the Si_3N_4 membrane, which could be further confirmed by TEM and HRTEM (Figure 6d–e). In addition, it can also be seen from Figure 6b that the separation layer of the amorphous silicon oxycarbide membrane supported by silicon nitride is dense, defect-free and has good adhesion to the support body, which will be demonstrated by long-term permeation measurements of H_2 and CO_2 [55]. The SAED image in Figure 6f also indicates that the SiOC membrane was amorphous, retaining the memory of the PSO gel [56]. Figure 6g–i show an EDS map of Figure 6c, indicating the uniform distribution of Si, O and C. The morphology of the membrane indicates that multiple spin-coating pyrolysis ensures the compactness of the SiOC membrane by eliminating the small pores during gel formation.

Figure 7a shows the nitrogen adsorption isotherm at -196 °C of the SiOC membrane obtained at 1000 °C. The low nitrogen adsorption capacity in the relative pressure range of 0.01 to 1.0 indicates that the SiOC membrane was non-porous, which may be caused by the compactness of the SiOC structure [31,53]. So, the permeance of gas through the membrane should obey a mechanism involving jumps between solubility sites for non-porous membranes [57].

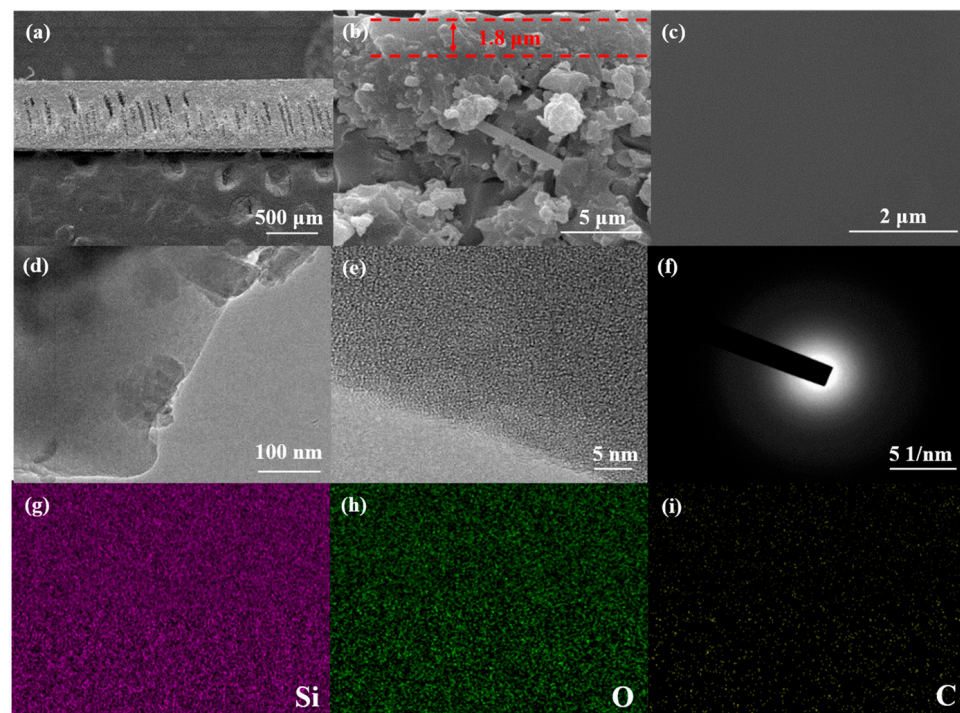


Figure 6. (a) Cross-section SEM of the SiOC membrane on the Si_3N_4 ceramic membrane; (b) fracture and (c) upper surface of the SiOC membrane; (d) TEM and (e) HRTEM of the SiOC membrane; (f) SAED of the SiOC membrane; and (g–i) EDS mapping of (c).

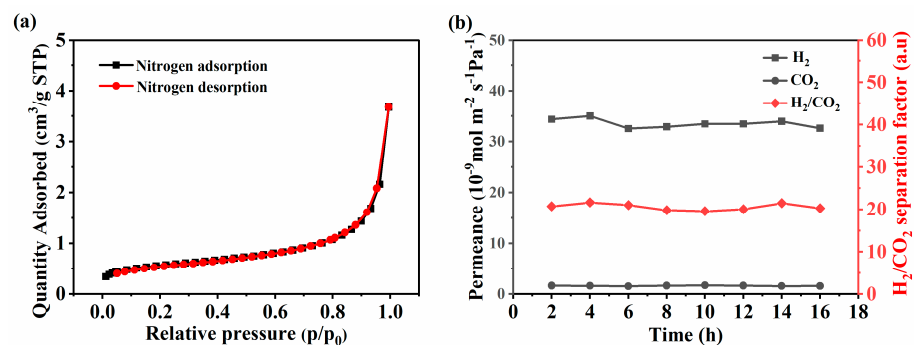


Figure 7. (a) Nitrogen adsorption and desorption isotherm of the SiOC membrane. (b) The gas permeability of H_2/CO_2 as a function of the penetration time.

3.2. Gas Separation Performance of Composite Membrane

Figure 7b shows the gas permeability as a function of the penetration time. The single gas permeability of H_2 (kinetic diameter 0.289 nm) and CO_2 (kinetic diameter 0.330 nm) was measured at 25 °C and 0.5 MPa. H_2 showed a stable H_2 permeation of $3.26 \times 10^{-8} \text{ mol m}^{-2} \text{ Pa}^{-1} \text{ s}^{-1}$, which is much higher than $1.61 \times 10^{-9} \text{ mol m}^{-2} \text{ Pa}^{-1} \text{ s}^{-1}$ for CO_2 . This also indicated that the synthesized membrane was very stable. The permeability of the gas depended mainly on the kinetic diameter of the gas rather than the molecular weight [14,21]. The ideal separation factor for H_2 and CO_2 was about 20, which was much higher than the corresponding ideal Knudsen diffusion selectivity (4.69), indicating that the membrane had molecular sieving behavior. The prepared SiOC membrane was compared in detail with the reported membranes, as shown in Table 1. It can be clearly seen that the SiOC membrane showed good selectivity. The good performance of the composite ceramic membrane could be attributed to the good compatibility between SiOC and silicon nitride and the formation of strong chemical bonds at the interface. Future research will

focus on regulating the structure to adapt to different gases and their separation ability at high temperatures.

Table 1. The ideal selectivity of the SiOC membrane in this work and various membranes previously reported.

Membrane	Base	Thickness (μm)	Temperature ($^{\circ}\text{C}$)	H_2 Permeability ($\text{mol m}^{-2} \text{Pa}^{-1}\text{s}^{-1}$)	Selectivity (H_2/CO_2)	Ref.
SiOC	Si_3N_4	~1.8	25	3.26×10^{-8}	~20	This work
SiOC	Al_2O_3	~0.3	300	1.78×10^{-8}	~10	[13]
BTESE	Al_2O_3	N/A	200	3.75×10^{-7}	7.3	[19]
MoS_2	Al_2O_3	0.06	35	8.21×10^{-7}	4.4	[21]
Zeolite	Al_2O_3	20~30	35	2.0×10^{-10}	24	[22]
SiOC	SiO_2	N/A	200	8.90×10^{-7}	<10	[31]
ZIF-8	Si_3N_4	>60	25	8.35×10^{-7}	~7.3	[36]

N/A relevant data are not available.

4. Conclusions

We used the spin-coating method to load the amorphous SiOC membrane on the Si_3N_4 membrane without using mesoporous materials as the transition layer. The prepared composite membrane showed good molecular sieving ability, which benefited from the dense SiOC ceramic membrane. The gas separation factor of H_2 and CO_2 was about 20, which is much higher than the Knudsen diffusion, 4.69. Therefore, SiOC ceramic membranes have a certain practicability for waste gas treatment and gas separation.

Author Contributions: Conceptualization, H.J. and X.X.; methodology, H.J. and X.X.; writing—original draft preparation, H.J.; writing—review and editing, X.X.; supervision, X.X. All authors have read and agreed to the published version of the manuscript.

Funding: This research was supported by the Anhui Provincial Natural Science Foundation (2308085ME139).

Institutional Review Board Statement: Not applicable.

Data Availability Statement: Data are contained within the article.

Conflicts of Interest: The authors declare no conflicts of interest.

References

- Stern, P.C.; Sovacool, B.K.; Dietz, T. Towards a science of climate and energy choices. *Nat. Clim. Chang.* **2016**, *6*, 547–555. [CrossRef]
- Møller, K.T.; Jensen, T.R.; Akiba, E.; Li, H.-W. Hydrogen—A sustainable energy carrier. *Prog. Nat. Sci.-Mater.* **2017**, *27*, 34–40. [CrossRef]
- Liu, W.; Zuo, H.; Wang, J.; Xue, Q.; Ren, B.; Yang, F. The production and application of hydrogen in steel industry. *Int. J. Hydrogen Energy* **2021**, *46*, 10548–10569. [CrossRef]
- Abe, J.O.; Popoola, A.P.I.; Ajenifuja, E.; Popoola, O.M. Hydrogen energy, economy and storage: Review and recommendation. *Int. J. Hydrogen Energy* **2019**, *44*, 15072–15086. [CrossRef]
- Li, L.; Lou, W.; Kong, L.; Shen, W. Hydrogen Commonly Applicable from Medicine to Agriculture: From Molecular Mechanisms to the Field. *Curr. Pharm. Des.* **2021**, *27*, 747–759. [CrossRef] [PubMed]
- Liu, J.; Tang, C.; Ke, Z.; Chen, R.; Wang, H.; Li, W.; Jiang, C.; He, D.; Wang, G.; Xiao, X. Optimizing Hydrogen Adsorption by d-d Orbital Modulation for Efficient Hydrogen Evolution Catalysis. *Adv. Energy Mater.* **2022**, *12*, 2103301. [CrossRef]
- Wang, F.; Wu, Y.; Dong, B.; Lv, K.; Shi, Y.; Ke, N.; Hao, L.; Yin, L.; Bai, Y.; Xu, X.; et al. Robust Porous WC-Based Self-Supported Ceramic Electrodes for High Current Density Hydrogen Evolution Reaction. *Adv. Sci.* **2022**, *9*, 2106029. [CrossRef] [PubMed]
- Jin, S.; Jing, H.; Wang, L.; Hu, Q.; Zhou, A. Construction and performance of $\text{CdS}/\text{MoO}_2/\text{Mo}_2\text{C}/\text{MXene}$ photocatalyst for H_2 production. *J. Adv. Ceram.* **2022**, *11*, 1431–1444. [CrossRef]
- Shi, Y.; Zheng, D.; Zhang, X.; Lv, K.; Wang, F.; Dong, B.; Wang, S.; Yang, C.; Li, J.; Yang, F.; et al. Self-Supported Ceramic Electrode of 1T-2H MoS_2 Grown on the TiC Membrane for Hydrogen Production. *Chem. Mater.* **2021**, *33*, 6217–6226. [CrossRef]
- Wang, F.; Dong, B.; Wang, J.; Ke, N.; Tan, C.; Huang, A.; Wu, Y.; Hao, L.; Yin, L.; Xu, X.; et al. Self-supported porous heterostructure WC/ WO_{3-x} ceramic electrode for hydrogen evolution reaction in acidic and alkaline media. *J. Adv. Ceram.* **2022**, *11*, 1208–1221. [CrossRef]

11. Mo, Z.; Yang, W.; Gao, S.; Shang, J.K.; Ding, Y.; Sun, W.; Li, Q. Efficient oxygen reduction reaction by a highly porous, nitrogen-doped carbon sphere electrocatalyst through space confinement effect in nanopores. *J. Adv. Ceram.* **2021**, *10*, 714–728. [[CrossRef](#)]
12. Dong, Y.S.L.J.; Kanezashi, M.; Tang, Z. Microporous inorganic membranes for high temperature hydrogen purification. *J. Appl. Phys.* **2008**, *104*, 121301. [[CrossRef](#)]
13. Prasad, R.M.; Jüttke, Y.; Richter, H.; Voigt, I.; Riedel, R.; Gurlo, A. Mechanism of Gas Separation through Amorphous Silicon Oxycarbide Membranes. *Adv. Eng. Mater.* **2016**, *18*, 721–727. [[CrossRef](#)]
14. Gu, Y.; Oyama, S.T. High Molecular Permeance in a Poreless Ceramic Membrane. *Adv. Mater.* **2007**, *19*, 1636–1640. [[CrossRef](#)]
15. Sircar, S.; Golden, T.C. Purification of Hydrogen by Pressure Swing Adsorption. *Sep. Sci. Technol.* **2000**, *35*, 667–687. [[CrossRef](#)]
16. Zhang, N.; Bénard, P.; Chahine, R.; Yang, T.; Xiao, J. Optimization of pressure swing adsorption for hydrogen purification based on Box-Behnken design method. *Int. J. Hydrogen Energy* **2021**, *46*, 5403–5417. [[CrossRef](#)]
17. Zhu, X.; Li, S.; Shi, Y.; Cai, N. Recent advances in elevated-temperature pressure swing adsorption for carbon capture and hydrogen production. *Prog. Energ. Combust.* **2019**, *75*, 100784. [[CrossRef](#)]
18. Iwamoto, Y. Precursors-Derived Ceramic Membranes for High-Temperature Separation of Hydrogen. *J. Ceram. Soc. Jpn.* **2007**, *115*, 947–954. [[CrossRef](#)]
19. Song, H.; Zhao, S.; Lei, J.; Wang, C.; Qi, H. Pd-doped organosilica membrane with enhanced gas permeability and hydrothermal stability for gas separation. *J. Mater. Sci.* **2016**, *51*, 6275–6286. [[CrossRef](#)]
20. Bernardo, G.; Araújo, T.; da Silva Lopes, T.; Sousa, J.; Mendes, A. Recent advances in membrane technologies for hydrogen purification. *Int. J. Hydrogen Energy* **2020**, *45*, 7313–7338. [[CrossRef](#)]
21. Ding, L.; Wei, Y.; Li, L.; Zhang, T.; Wang, H.; Xue, J.; Ding, L.-X.; Wang, S.; Caro, J.; Gogotsi, Y. MXene molecular sieving membranes for highly efficient gas separation. *Nat. Commun.* **2018**, *9*, 155. [[CrossRef](#)]
22. Ockwig, N.W.; Nenoff, T.M. Membranes for hydrogen separation. *Chem. Rev.* **2007**, *107*, 4078–4110. [[CrossRef](#)]
23. Uemiyama, S. Brief Review of Steam Reforming Using a Metal Membrane Reactor. *Top. Catal.* **2004**, *29*, 79–84. [[CrossRef](#)]
24. Park, H.B.; Kamcev, J.; Robeson, L.M.; Elimelech, M.; Freeman, B.D. Maximizing the right stuff: The trade-off between membrane permeability and selectivity. *Science* **2017**, *356*, 1137. [[CrossRef](#)]
25. Luis, P.; Van Gerven, T.; Van der Bruggen, B. Recent developments in membrane-based technologies for CO₂ capture. *Prog. Energ. Combust.* **2012**, *38*, 419–448. [[CrossRef](#)]
26. Sholl, D.S.; Lively, R.P. Seven chemical separations to change the world. *Nature* **2016**, *532*, 435–437. [[CrossRef](#)]
27. Gin, D.L.; Noble, R.D. Designing the Next Generation of Chemical Separation Membranes. *Science* **2011**, *332*, 674–676. [[CrossRef](#)]
28. Amin, M.; Butt, A.S.; Ahmad, J.; Lee, C.; Azam, S.U.; Mannan, H.A.; Naveed, A.B.; Farooqi, Z.U.R.; Chung, E.; Iqbal, A. Issues and challenges in hydrogen separation technologies. *Energy Rep.* **2023**, *9*, 894–911. [[CrossRef](#)]
29. Kim, H.W.; Yoon, H.W.; Yoon, S.M.; Yoo, B.M.; Ahn, B.K.; Cho, Y.H.; Shin, H.J.; Yang, H.; Paik, U.; Kwon, S.; et al. Selective Gas Transport Through Few-Layered Graphene and Graphene Oxide Membranes. *Science* **2013**, *342*, 91–95. [[CrossRef](#)] [[PubMed](#)]
30. Shen, J.; Liu, G.; Huang, K.; Chu, Z.; Jin, W.; Xu, N. Subnanometer Two-Dimensional Graphene Oxide Channels for Ultrafast Gas Sieving. *Acs Nano* **2016**, *10*, 3398–3409. [[CrossRef](#)] [[PubMed](#)]
31. Inde, H.; Kanezashi, M.; Nagasawa, H.; Nakaya, T.; Tsuru, T. Tailoring a Thermally Stable Amorphous SiOC Structure for the Separation of Large Molecules: The Effect of Calcination Temperature on SiOC Structures and Gas Permeation Properties. *ACS Omega* **2018**, *3*, 6369–6377. [[CrossRef](#)]
32. Alaslai, N.; Ghanem, B.; Alghunaimi, F.; Pinnau, I. High-performance intrinsically microporous dihydroxyl-functionalized triptycene-based polyimide for natural gas separation. *Polymer* **2016**, *91*, 128–135. [[CrossRef](#)]
33. Do, Y.S.; Seong, J.G.; Kim, S.; Lee, J.G.; Lee, Y.M. Thermally rearranged (TR) poly(benzoxazole-co-amide) membranes for hydrogen separation derived from 3,3'-dihydroxy-4,4'-diamino-biphenyl (HAB), 4,4'-oxydianiline (ODA) and isophthaloyl chloride (IPCl). *J. Membr. Sci.* **2013**, *446*, 294–302. [[CrossRef](#)]
34. Orme, C.J.; Stone, M.L.; Benson, M.T.; Peterson, E.S. Testing Of Polymer Membranes For The Selective Permeability Of Hydrogen. *Sep. Sci. Technol.* **2003**, *38*, 3225–3238. [[CrossRef](#)]
35. Perry, J.D.; Nagai, K.; Koros, W.J. Polymer Membranes for Hydrogen Separations. *Mrs. Bull.* **2011**, *31*, 745–749. [[CrossRef](#)]
36. Wang, J.-W.; Li, N.-X.; Li, Z.-R.; Wang, J.-R.; Xu, X.; Chen, C.-S. Preparation and gas separation properties of Zeolitic imidazolate frameworks-8 (ZIF-8) membranes supported on silicon nitride ceramic hollow fibers. *Ceram. Int.* **2016**, *42*, 8949–8954. [[CrossRef](#)]
37. Hamid, M.R.A.; Yaw, T.C.S.; Tohir, M.Z.M.; Ghani, W.A.W.A.K.; Sutrisna, P.D.; Jeong, H.-K. Zeolitic imidazolate framework membranes for gas separations: Current state-of-the-art, challenges, and opportunities. *J. Ind. Eng. Chem.* **2021**, *98*, 17–41. [[CrossRef](#)]
38. Mirqasemi, M.S.; Homayoonfal, M.; Rezakazemi, M. Zeolitic imidazolate framework membranes for gas and water purification. *Environ. Chem. Lett.* **2019**, *18*, 1–52. [[CrossRef](#)]
39. Jia, M.; Zhang, X.-F.; Feng, Y.; Zhou, Y.; Yao, J. In-situ growing ZIF-8 on cellulose nanofibers to form gas separation membrane for CO₂ separation. *J. Membr. Sci.* **2020**, *595*, 117579. [[CrossRef](#)]
40. Zhang, Q.; Hou, Q.; Huang, G.; Fan, Q. Removal of heavy metals in aquatic environment by graphene oxide composites: A review. *Environ. Sci. Pollut. Res.* **2019**, *27*, 190–209. [[CrossRef](#)] [[PubMed](#)]
41. Gu, Q.; Kotobuki, M.; Kirk, C.H.; He, M.; Lim, G.J.H.; Ng, T.C.A.; Zhang, L.; Ng, H.Y.; Wang, J. Overcoming the Trade-off between Water Permeation and Mechanical Strength of Ceramic Membrane Supports by Interfacial Engineering. *ACS Appl. Mater. Interfaces* **2021**, *13*, 29199–29211. [[CrossRef](#)] [[PubMed](#)]

42. Zhang, Z.; Yu, H.; Xu, M.; Cui, X. Preparation, characterization and application of geopolymer-based tubular inorganic membrane. *Appl. Clay Sci.* **2021**, *203*, 106001. [[CrossRef](#)]
43. Bechstedt, P.K.F.; Zywietz, A.; Karch, K.; Adolph, B.; Tenelsen, K.; Furthmüller, J. Polytypism and Properties of Silicon Carbide. *Phys. Status Solidi (b)* **1997**, *202*, 35–62. [[CrossRef](#)]
44. Hasegawa, G.; Kanamori, K.; Nakanishi, K.; Hanada, T. Fabrication of macroporous silicon carbide ceramics by intramolecular carbothermal reduction of phenyl-bridged polysilsesquioxane. *J. Mater. Chem.* **2009**, *19*, 7716. [[CrossRef](#)]
45. Yu, Z.; Chen, T.; Du, H.; Li, F.; Zhu, Q. Single-source-precursor derived SiOC ceramics with in-situ formed CNTs and core-shell structured CoSi@C nanoparticles towards excellent electromagnetic wave absorption properties. *J. Adv. Ceram.* **2023**, *12*, 1119–1135. [[CrossRef](#)]
46. Yan, X.; Su, D.; Han, S. Phase separation induced macroporous SiOC ceramics derived from polysiloxane. *J. Eur. Ceram. Soc.* **2015**, *35*, 443–450. [[CrossRef](#)]
47. Blum, Y.; Sorarù, G.D.; Ramaswamy, A.P.; Hui, D.; Carturan, S.M.; Riedel, R. Controlled Mesoporosity in SiOC via Chemically Bonded Polymeric “Spacers”. *J. Am. Ceram. Soc.* **2013**, *96*, 2785–2792. [[CrossRef](#)]
48. Dong, B.-B.; Wang, F.-H.; Yang, M.-Y.; Yu, J.-L.; Hao, L.-Y.; Xu, X.; Wang, G.; Agathopoulos, S. Polymer-derived porous SiOC ceramic membranes for efficient oil-water separation and membrane distillation. *J. Membr. Sci.* **2019**, *579*, 111–119. [[CrossRef](#)]
49. Dong, B.; Han, Y.; Wang, T.; Lei, Z.; Chen, Y.; Wang, F.; Abadikhah, H.; Khan, S.A.; Hao, L.; Xu, X.; et al. Hard SiOC Microbeads as a High-Performance Lithium-Ion Battery Anode. *ACS Appl. Energy Mater.* **2020**, *3*, 10183–10191. [[CrossRef](#)]
50. Guo, F.; Su, D.; Liu, Y.; Wang, J.; Yan, X.; Chen, J.; Chen, S. High acid resistant SiOC ceramic membranes for wastewater treatment. *Ceram. Int.* **2018**, *44*, 13444–13448. [[CrossRef](#)]
51. Wang, J.W.; Li, L.; Gu, J.Q.; Yang, M.Y.; Xu, X.; Chen, C.S.; Wang, H.T.; Agathopoulos, S. Highly stable hydrophobic SiNCO nanoparticle-modified silicon nitride membrane for zero-discharge water desalination. *AIChE J.* **2016**, *63*, 1272–1277. [[CrossRef](#)]
52. Zhao, W.; Zhang, S.; Zhang, Y.; Li, S.; Liu, X.; He, C.; Zheng, Z.; Hou, J. Environmentally Friendly Solvent-Processed Organic Solar Cells that are Highly Efficient and Adaptable for the Blade-Coating Method. *Adv. Mater.* **2017**, *30*, 1704837. [[CrossRef](#)] [[PubMed](#)]
53. Du, B.; Hong, C.; Wang, A.; Zhou, S.; Qu, Q.; Zhou, S.; Zhang, X. Preparation and structural evolution of SiOC preceramic aerogel during high-temperature treatment. *Ceram. Int.* **2018**, *44*, 563–570. [[CrossRef](#)]
54. Gontarek-Castro, E.; Di Luca, G.; Lieder, M.; Gugliuzza, A. Graphene-Coated PVDF Membranes: Effects of Multi-Scale Rough Structure on Membrane Distillation Performance. *Membranes* **2022**, *12*, 511. [[CrossRef](#)]
55. Tseng, H.-H.; Wang, C.-T.; Zhuang, G.-L.; Uchytel, P.; Reznickova, J.; Setnickova, K. Enhanced H₂/CH₄ and H₂/CO₂ separation by carbon molecular sieve membrane coated on titania modified alumina support: Effects of TiO₂ intermediate layer preparation variables on interfacial adhesion. *J. Membr. Sci.* **2016**, *510*, 391–404. [[CrossRef](#)]
56. Tian, J.; Thallapally, P.K.; Dalgarno, S.J.; McGrail, P.B.; Atwood, J.L. Amorphous Molecular Organic Solids for Gas Adsorption. *Angew. Chem. Int. Ed.* **2009**, *48*, 5492–5495. [[CrossRef](#)]
57. Oyama, S.; Lee, D.; Hacırlıoğlu, P.; Saraf, R. Theory of hydrogen permeability in nonporous silica membranes. *J. Membr. Sci.* **2004**, *244*, 45–53. [[CrossRef](#)]

Disclaimer/Publisher’s Note: The statements, opinions and data contained in all publications are solely those of the individual author(s) and contributor(s) and not of MDPI and/or the editor(s). MDPI and/or the editor(s) disclaim responsibility for any injury to people or property resulting from any ideas, methods, instructions or products referred to in the content.